

Trapping of electromagnetic waves by two dimensional plasma-metamaterial composite structures

D. Tsiklauri^{id} * and I. Morrison^{id}

*Joule Physics Laboratory, School of Science, Engineering and Environment,
University of Salford, Manchester, M5 4WT, United Kingdom*

(Dated: October 10, 2024)

In this work we (i) extend previous 1D studies of electromagnetic (EM) wave propagation in an over-dense plasma-metamaterial composite into two spatial dimensions and (ii) study trapping of EM waves by the composite 2D structures (barriers). Such barriers are formed when metamaterial spatially co-exists with a plasma density depletion in a form of a slab or two-dimensional density rectangular depletions (DRDs). This is analogous to EM wave trapping by preformed density cavities in near-critical density plasmas, studied before. We find that plasma-metamaterial composite allows to trap EM waves by both slab and DRD configurations, thus forming a standing wave at the edge of an opaque region. The standing wave subsequently damps which offers applications such as heat deposition or substrate materials (micro)machining depending on EM wave intensity. The established results may find future applications such as: more efficient plasma vapour deposition, controlling EM wave propagation (EM wave trapping) in invisibility cloaks and alike. The EM wave trapping conditions are elucidated by a set of particle-in-cell (PIC) numerical simulations.

I. INTRODUCTION

Ref. [1] gives a good background and lays a foundation to the considered research. It is well-known that industrial applications such as vapor deposition, material surface treatment and many others use plasma as an agent or a means of delivery [2]. Generally, physical vapor deposition (PVD) is a method in-vacuum deposition that is used to produce thin films and coatings. PVD's main feature is that material changing from a condensed phase to a vapor phase and then back to a thin film condensed phase. Common PVD processes are sputtering and evaporation. PVD is used in the manufacture of items which require thin films for mechanical, optical, chemical or electronic functions. Examples include semiconductor devices such as thin film solar panels [3], aluminized PET film for food packaging and balloons [4], and titanium nitride coated cutting tools for metalworking. Besides PVD tools for fabrication, special smaller tools (mainly for scientific purposes) have been developed [5]. Inside the Plasma Spray-Physical Vapor Deposition, or PS-PVD, ceramic powder is introduced into the plasma flame, which vaporizes it and then condenses it on the (cooler) workpiece to form the ceramic coating. Some examples of PVD include (i) Pulsed laser deposition: In which a high-power laser ablates material from the target into a vapor; (ii) Sputter deposition: In which a glow plasma discharge (usually localized around the "target" by a magnet) bombards the material sputtering some away as a vapor for subsequent deposition; (iii) Pulsed electron deposition: In which a highly energetic pulsed electron beam ablates material from the target generating a plasma stream under non-equilibrium conditions. PS-PVD, is a unique technology that enables highly tailorable functional films and coatings with various rare metal elements to be processed. This technology bridges the gap between conventional thermal spray and vapor deposition and provides a variety of coating microstructures composed of vapor, liquid, and solid deposition units.

A common method of creation of plasma in these applications is gas irradiation by microwaves. Microwaves are a form of electromagnetic radiation with frequency range between 1 and 100 GHz (wavelengths between 300 and 3 mm). When a microwave enters a vessel with the plasma discharge, and the electron density n_e is larger than the cut-off density for the incident microwave, the latter cannot propagate through plasma and is confined to its surface [6]. In microwaves, the surface wave, with a typical width of electron inertial length c/ω_{pe} , sustains the over-dense plasma, but the width of the generated plasma is narrow. In order to increase penetration of microwaves into the over-dense plasma, DC magnets or magnetic field coils are used. The magnetized plasma has the propagation band under the electron cyclotron frequency, and this enables to optimize this frequency by the strength of the external magnetic field. This propagation mode is the whistler mode, and a wavenumber becomes infinity when the incident wave frequency approaches the electron cyclotron frequency. The electron cyclotron resonance (ECR) heating is useful for the efficient power injection into the overdense plasma, but it is difficult to prepare a large-scale DC magnet for the plasma generation systems. Metamaterials are artificial composites made of unit patterns whose size is much smaller than the wavelength of the corresponding waves. Metamaterials give the extraordinary propagation of EM waves and it cannot occur in natural materials. Refractive index N becomes negative in metamaterials because both permittivity ϵ and permeability μ become negative [7]. The experimental verification was performed with the combination of the split-ring resonators (SRRs) as negative- μ metamaterials [8]. Theoretical and numerical simulation studies of wave propagation in negative N are numerous [9–11].

Refs. [11, 12] reported the generation of the second harmonic waves in negative N with quadratic nonlinear response. Also the nonlinear frequency conversion process was demonstrated to be analogous to non-linear optics [13]. Also, experimental studies were performed with the combination of the arrays of metal wires as a negative- ϵ material [14–16]. The array of metal wires has a cut-off frequency and acquires negative ϵ under the cut-off frequency as in the over-dense

* D.Tsiklauri@salford.ac.uk

plasma [17]. A composite of an overdense plasma and a negative- μ metamaterial has been investigated experimentally [18–20] and by means of numerical simulations [21, 22]. It was demonstrated that that refractive index N was negative, the second harmonic wave was present in Ref. [19], and SRRs were electrically connected with plasma at a microscopic level [20], wave propagation was not clearly confirmed in the composite of an overdense plasma and a negative- μ metamaterial. Ref.[1] conducted 1D electromagnetic PIC simulations of EM wave propagation in the composite of overdense plasma and the negative- μ metamaterial. In their simulation EM waves enter the plasma-metamaterial composite, and propagate in it with a negative phase velocity and a positive group velocity. This way, Ref.[1] confirmed that the plasma-metamaterial composite has a negative refractive index. Ref. [23] gives an up-to-date background to the experimental implementation of the considered research.

Ref.[21] performed FDTD simulations and reported the wave propagation with a negative N in the array of plasma columns under a negative- μ state. They assume that a propagating microwave contributes to simultaneous plasma generation by its electric field E that deforms ϵ and refractive index N in the metamaterial; this is a field-dependent metamaterial, in which a propagating wave conversely suffers from the changes of ϵ and/or N , where E , ϵ , and N settle self-consistently. Such a metamaterial may exhibit nonlinear features due to its field-dependent properties. Ref.[22] studied the local electromagnetic fields around an SRR when a plasma exists near the SRR. Since both reports used the FDTD solver to simulate EM wave coupling to plasmas i.e. coupling between high-frequency EM waves and the plasma occurs mainly via the electron current density (ions are heavy enough not to respond in EM field variations). Hence in both Ref.[21] and Ref.[22] the kinetic effects such as self-consistent EM fields from collection of billions of particles in plasma were not considered. These effects must be included in the case when a high-power electromagnetic wave enters the overdense plasma under a negative- μ state.

Although, Ref.[1] conducted fully kinetic electromagnetic PIC simulations of EM wave propagation in the composite of overdense plasma and the negative- μ metamaterial, they used PIC code modified from KEMPO1 which is *spatially 1 dimensional (1D)*. There is a clear need to extend model of Ref. [1] beyond simple 1D case. This has very strong industrial applications in plasma processing. i.e. use of negative- μ metamaterial (the plasma-metamaterial composite) will enable to increase plasma density which is crucial for plasma processing efficiency. It can be also related to modern applications such as ion thrusters and plasma based acceleration, intense X-Ray sources etc. Typical microwaves used today have frequencies in the few GHz range and the cut-off density that corresponds to the cut-off frequency $f_{pe} = \omega_{pe}/2\pi$ is few 10^{16} m^{-3} . If this density can be increased then plasma processing will become more efficient, as the reaction rate is usually proportional to the product of number densities of the reactant species. Thus, in this work propose to extend previous 1D results [1] into two spatial dimensions and use the modified 2D (and in the future 3D) EPOCH PIC code [24]. The key novelty is that we

propose to use much more general, fully kinetic regime using EPOCH code, while all previous research [21, 22] used FTDT method to simulate plasmas, hence kinetic effects of a plasma and non-linearity were not considered. These effects must be included when a high-power EM wave enters the overdense plasma under a negative- μ state.

The second input and motivation for the present study comes from research related to the trapping of EM waves in preformed density cavities in near-critical density plasmas [25–29]. In a more broader context, the present research is about an ability to control and manipulate EM radiation by means of combining the presence of plasma and metamaterials. In particular Ref. [29] studied EM wave trapping in cavities in near-critical density plasmas using 2D particle-in-cell (PIC) simulation. They find that in plasma, laser’s ponderomotive force can create a vacuum cavity bounded by a thin overcritical-density wall. The EM waves are self-consistently trapped as a half-cycle electromagnetic wave in the form of an oscillon-caviton structure. Further, the trapped EM wave is slowly depleted through interaction with the cavity wall. Ref. [29] also studied a situation when a near-critical density plasma contains a *preformed* density cavity and found that EM wave becomes trapped, forming a standing wave. They find that the trapped light is characterized as multi-peak structure and that the overdense plasma layer formed around the self-generated and preformed cavities that is induced by the laser ponderomotive force is the natural reason for EM wave trapping. Ref. [29] also discusses possible applications of the EM wave trapping in preformed and self-consistently generated by EM wave’s ponderomotive force density cavities in near-critical density plasmas.

We close the introduction by stating the aims of this work that are two-fold: (i) to extend previous one dimensional studies of electromagnetic (EM) wave propagation on an overdense plasma-metamaterial [1] composite into two spatial dimensions and (ii) to study trapping of EM waves by the composite barriers in analogy with their trapping in preformed density cavities in near-critical density plasmas [29]. We therefore propose to use modified 2D EPOCH code, as described in section 2.

II. THE MODEL

We modify the existing state-of-the-art, fully kinetic, explicit, electromagnetic, 2D, particle-in-cell (PIC) code called EPOCH [24]. The modification is by adding the effect of negative- μ metamaterial (the plasma-metamaterial composite) via adding the magnetic current term, \mathbf{J}_m , to the relevant Maxwell’s equation as following:

$$\nabla \times \mathbf{E} = -\mathbf{J}_m - \frac{\partial \mathbf{B}}{\partial t}, \quad (1)$$

$$\frac{\partial \mathbf{J}_m}{\partial t} = \omega_m^2 \mathbf{B}, \quad (2)$$

where ω_m is the magnetic resonance frequency. The modification of EPOCH code is insertion of \mathbf{J}_m . The metamaterial effect, based on \mathbf{J}_m , does not affect both electric field,

\mathbf{E} , and plasma in this simulation. \mathbf{J}_m is determined only by \mathbf{B} and the constant value of ω_m . Such approach has proven to be very effective in modeling of bulk effects of negative- μ metamaterial (see Ref.[1] for details). The plane, linearly-polarized EM wave is excited by the external current \mathbf{J}_s at $x = 1\Delta$, the first grid point of the simulation domain, where $\Delta = r_D = \sqrt{\epsilon_0 k_B T_e / (n_e q_e^2)}$ is the Debye length. \mathbf{J}_s oscillates in vertical z -direction $\mathbf{J}_s = \hat{z} J_z = J_0 \sin(\omega_0 t)$. EM wave travels in x -direction and has components E_z and B_y as it travels initially in free-space. The plasma-metamaterial composite exists in the region where $12.8 < x < 25.6$, see Figure 2(a), that we call *plasma region*. Note that spatial dimensions are normalized by the EM wave inertial length c/ω_0 . When EM wave enters the plasma region it excites a different current \mathbf{J}_p (subscript p stands for plasma), which is prescribed by the following equations:

$$\nabla \times \mathbf{B} = \mu_0 \mathbf{J}_p + \mu_0 \epsilon_0 \frac{\partial \mathbf{E}}{\partial t}, \quad (3)$$

$$\frac{d\gamma v_\alpha}{dt} = \frac{q_\alpha}{m_\alpha} (\mathbf{E} + \mathbf{v}_\alpha \times \mathbf{B}), \quad (4)$$

where \mathbf{J}_p in equation (3) is different from the initial \mathbf{J}_s because when EM wave enters plasma-metamaterial composite, electrons and ions start to oscillate and \mathbf{J}_p is now prescribed by dielectric response of plasma and velocity of oscillating plasma particles of species α , \mathbf{v}_α . Note that when EM wave amplitude and/or plasma number density are small, plasma has the simple dispersive back-reaction to EM wave's \mathbf{E} as $\partial \mathbf{J}_p / \partial t \simeq \omega_{pe}^2 \mathbf{E}$ where ω_{pe} is the plasma frequency. When metamaterial is present its effect is felt by resonant interaction of EM wave's magnetic field \mathbf{B} . The effect of magnetic resonance can be described by appearance of another frequency ω_m , which appears in equation (2). Note that in equation (2), the term $\partial \mathbf{J}_m / \partial t = \omega_m^2 \mathbf{B}$ is mathematically similar to $\partial \mathbf{J}_p / \partial t \simeq \omega_{pe}^2 \mathbf{E}$. This effectively means that presence of metamaterial is manifest by additional current \mathbf{J}_m . In this formulation, the metamaterial does not affect \mathbf{E} and plasma in this simulation. \mathbf{J}_m is determined only by \mathbf{B} and the constant ω_m . Note that plasma current \mathbf{J}_p is prescribed by nonlinear and kinetic motions of the particles and consists of the x - and z -axis components. The magnetic current density \mathbf{J}_m is parallel to \mathbf{B} and consists of the y -axis component. Therefore effective permittivity of the plasma ϵ_p and the effective permeability of the metamaterial μ_m are expressed as $\epsilon_p = 1 - \omega_{pe}^2 / \omega_0^2$ and $\mu_m = 1 - \omega_m^2 / \omega_0^2$. This implies that is EM wave's frequency ω_0 is smaller than both ω_{pe} and ω_m ($\omega_0 < \omega_{pe}$ and $\omega_0 < \omega_m$) thus both ϵ_p and μ_m are negative. Therefore, refractive index $N = \sqrt{\epsilon_p \mu_m} = i^2 \sqrt{|\epsilon_p| |\mu_m|} = -\sqrt{|\epsilon_p| |\mu_m|}$ becomes negative with all of the above described consequences such as EM wave's negative phase speed propagation in an over-dense plasma-metamaterial composite region [1].

The numerical recipe how to add the additional term responsible for the presence of the metamaterials is given in appendix A. Here we focus on the details of the numerical simulation set up. We aim using periodic boundary conditions throughout this work, which means that the solution

TABLE I: Table of numerical runs considered. See text discussing Fig.3 for the explanation of the notation used.

Case	$n_{e,i}(x)$	Grid $n_x \times n_y$	Metamat.	F
1a	$10^{-2} n_0$	8192×3	N	-
1b	Eq.(5)	8192×3	N	-
1c	$10^{-2} n_0$	8192×3	Y	-
1d	Eq.(5)	8192×3	Y	-
2	Eq.(5)	8192×128	Y	-
3	Eq.(7)	8192×128	Y	0.20
4	Eq.(7)	8192×128	Y	0.99
5	Eq.(8)	8192×128	Y	0.20
6	Eq.(8)	8192×128	Y	0.99

that is generated at $x = 1\Delta$, the first grid cell, that travels to the left, i.e. negative x -direction, and re-enters the simulation domain from the far right side of the domain $x = x_{\max}$, should not collide with the main studied numerical solution that travels in positive x -direction. This is achieved by the setting $x = x_{\max} = 8192\Delta$. It can be seen from Fig.1(a) that the left- and right- going numerical solutions never collide. The above defined notation for the Debye length can be also written as $\Delta = \lambda_D = v_{th,e} / \omega_{pe} = \sqrt{k_B T_{e,\max} / m_e} / \omega_{pe}$. Maximal temperature is set as $T_{e,\max} = m_e (0.0375c)^2 / k_B$. We use the term maximal temperature because it actually varies across x -axis. This is because as in Ref.[30] we keep pressure balance by making $p_{e,i} = n_{e,i}(x) k T_{e,i}(x) = const$, i.e. $T_{e,i}(x) = T_{e,i,\max} [n_0 / n_{e,i}(x)] \propto 1 / n_{e,i}(x)$. This ensures that the total initial pressure balance $p_{e,i} = const$ is fulfilled. n_0 is the background plasma number density, which is the same both for electrons and protons. The proton to electron mass ratio is set to the realistic value of 1836. The number densities $n_{e,i}$ and grid sizes are varied in different numerical runs as specified in Table I.

In EPOCH code physical quantities are in SI units, so we fix $n_0 = 10^{15}$ particles per m^{-3} typical of many laboratory (and accidentally astrophysical plasmas too). In cases 1a or 1c electron and ion number densities are set to $10^{-2} n_0$ particles per m^{-3} . The factor 10^{-2} , while drops number density to nearly zero, stops EPOCH from slowing down for numerical reasons. So effectively the cases with the constant values of $10^{-2} n_0$ or other spatial locations, when number density is varying, can be referred to as 'no plasma', i.e. effectively a vacuum.

We use 100 particles per cell for each species, so in total, in the large runs, we have $2 \times 100 \times 8192 \times 128 = 2.1 \times 10^8$ particles. One numerical run takes circa 2 days, 4 hours and 20 minutes on 8 processor cores of the 40-core Intel(R) Xeon(R) CPU E5-2630, 2.20GHz Linux server. We checked numerical convergence of the presented results. Twice coarser grid and twice less number of particles yields numerical results which look the same at plotting accuracy i.e. 1 %. The length is normalized on c/ω_0 . The end simulation time is set $t_{\text{end}} = 100/\omega_0$. Note that electron inertial length, c/ω_{pe} , is resolved with 27 grid points, i.e. $(c/\omega_{pe})/\Delta = 26.67$, while "EM wave" inertial length (this is not an accepted terminology), c/ω_0 , is resolved with 40 grid points, i.e. $(c/\omega_0)/\Delta = 40$. This means that the numerical resolution used is appropriate to resolve the

smallest relevant electron kinetic scales considered. In all our time-distance plots in figures 1-6 we use 500 time snapshots, which means that data is stored every $\Delta t = 0.2/\omega_0$. This ensures smoothness of the time-distance plots.

The electron and ion number densities are set using EPOCH's conditional function called $\text{if}(a, b, c)$. If a condition is *true*, the function returns b , otherwise the function returns c . For example, in the case 1b or 1d we set electron and ion number densities using

$$n_{e,i}(x) = \text{if} [(x < 512/n_x x_{\max}) \text{ or } (x > 1024/n_x x_{\max}), 10^{-2}n_0, n_0], \quad (5)$$

which means that this conditional function returns the following expression

$$n_{e,i} = \begin{cases} 10^{-2}n_0, & \text{if } (x < 512/n_x x_{\max}) \text{ or } (x > 1024/n_x x_{\max}) \\ n_0, & \text{otherwise.} \end{cases} \quad (6)$$

Note EPOCH maths parser uses *lt* instead of $<$ and *gt* instead of $>$ signs, see EPOCH user manual section 3.19 for details. In cases 1b or 1d the number density (given by equation(5)) is similar to case 2 (figure 2(a)), but in case 1b or 1d has $n_y = 3$, while for case 2 we set $n_y = 128$. Number density at time zero is plotted in case 2 only (figure 2(a)). Essentially this is a slab of plasma with top hat density of $n_0 = 10^{15} \text{ m}^{-3}$ between 512 and 1024 grid points in x -direction, while on domain edges number density drops to $10^{-2}n_0$. For the case 2 we use number density given by equation (5). For the cases 3 and 4 the number density used is given by equation (7)

$$n_{e,i}(x) = \text{if} [(x < 512/n_x x_{\max}) \text{ or } (x > 1024/n_x x_{\max}), 10^{-2}n_0, n_0] - F \times \text{if} [(x > 896/n_x x_{\max}) \text{ or } (x < 640/n_x x_{\max}), 0, n_0]. \quad (7)$$

This means that we subtract $F \times n_0$ in the region between 640 and 896 grid points in x -direction. Quantity $1 - F \times n_0$ is the plasma minimal number density in the slab. Note that for case 3, $F = 0.2$ and for case 4, $F = 0.99$, respectively. An explanation for the factor F will be given below after the EM wave driving will be specified. Number densities for the cases 3 and 4 graphically are shown in figures 3(a) and 4(a), respectively.

For the cases 5 and 6 the number density used is given by equation(8)

$$n_{e,i}(x, y) = \text{if} [(x < 512/n_x x_{\max}) \text{ or } (x > 1024/n_x x_{\max}), 10^{-2}n_0, n_0] \times \left(1 - F \times \left[e^{-(y-24/n_y y_{\max})^8/L_y^8} + e^{-(y-64/n_y y_{\max})^8/L_y^8} + e^{-(y-104/n_y y_{\max})^8/L_y^8} \right] \times e^{-(x-768/n_x x_{\max})^8/L_x^8} \right), \quad (8)$$

where $L_y = y_{\max}/10$ and $L_x = x_{\max}/64$ are the width of density structures and y - and x -directions. Number densities

for the cases 5 and 6 are plotted in figures 5(a) and 6(a), respectively. In equation (8) for case 5 we set $F = 0.2$ and for case 6 it is set to $F = 0.99$, respectively. Note that 768th grid is right in the middle between 512 and 1024 grid points in x -direction. This is the interval where both plasma and metamaterial are present in the cases 5 and 6.

With number densities in all numerical runs specified, next we describe how we generate (drive) EM waves. Similar to [1] we drive $x = 1\Delta$ cell as described in Appendix A. Here we only need to explain the driving field amplitude $E_0 = 760199.13 \text{ V m}^{-1}$, which produces linearly polarized in z -direction EM wave that propagates in both positive and negative x -directions. Note that because of periodic boundary conditions used, left propagating wave (i.e one that travels in the negative x -direction), re-enters the simulation domain from the right edge of the domain, as shown in figure 1(a). We also need to comment on the frequency $\omega_0 = 1.1893397 \times 10^9 \text{ Hz}$ radian. Firstly, E_0 is set to $E_0 = 0.25\omega_{pe}m_e c/q_e = 760199.13 \text{ V m}^{-1}$. The relevant electric field scale in this context is so called wave breaking electric field. The relevant parameter is $a = q_e E_0/(m_e \omega_0 c)$ [31]. When $a \geq 1$, the electron quiver motion is relativistic and the EM-plasma interaction is non-linear (wave breaks, i.e. over-turns due to non-linearity). EM wave stays linear otherwise for $a \leq 1$. For our value of E_0 used $a = 0.375$, which means our results stay in the moderately linear regime. Secondly, we set $\omega_0 = \omega_{pe}/1.5 = 1.1893397 \times 10^9 \text{ Hz}$ rad. This means that EM wave cannot propagate through plasma having number density $n_0 = 10^{15} \text{ particles per m}^{-3}$, as ω_0 is a factor of 1.5 below the plasma frequency.

We now can explain the use of $F = 0.2$ and $F = 0.99$ factors in equations (7) and (8) (see also table I). $(1 - F) \times 1.5 = 1.2$ for $F = 0.2$ and $(1 - F) \times 1.5 = 0.015$ for $F = 0.99$. In the first case ($(1 - F) \times 1.5 = 1.2$) plasma metamaterial composite is *transparent* to EM wave with negative phase speed propagation, while in the second case ($(1 - F) \times 1.5 = 0.015$) plasma metamaterial composite is *opaque* to EM wave.

III. THE RESULTS

In is section we present the results of our numerical simulations detailed in table I. We also provide justification for the above number density expressions used.

One of the aims of this work is to extend previous one dimensional studies of EM wave propagation on an over-dense plasma-metamaterial [1] composite into two spatial dimensions. This is achieved in 4 numerical runs for cases 1a, 1b, 1c and 1d, see table I for details. EPOCH 2D was modified as explained in Appendix A. The numerical grid is essentially one dimensional: $n_x \times n_y = 8192 \times 3$. This is because EPOCH 2D needs at least 3 grid points in y -direction. 8192 number of grids in x -direction was chosen so that left- and right-propagating EM waves, due to periodic boundary conditions, do not collide by the end simulation time of $t_{\text{end}} = 100/\omega_{pe}$. This is clearly seen in figure 1(a), where we show time-distance plot of $E_z(x, y = y_{\max}/2, t)/E_0$ when electron and ion number densities are set to $10^{-2}n_0$, i.e. essentially plasma is so thin, it can be regarded as a vacuum. Figure 1(a) corresponds to case 1a.

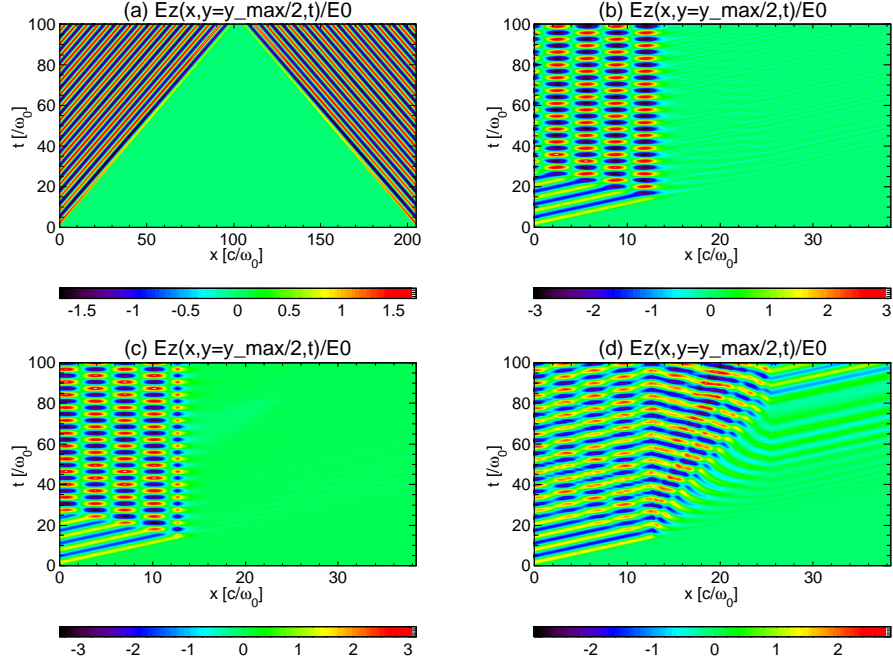


FIG. 1: Time-distance plot of $E_z(x, y = y_{\max}/2, t)/E_0$. (a) case 1a, (b) case 1b, (c) case 1c and (d) case 1d. See table I for details.

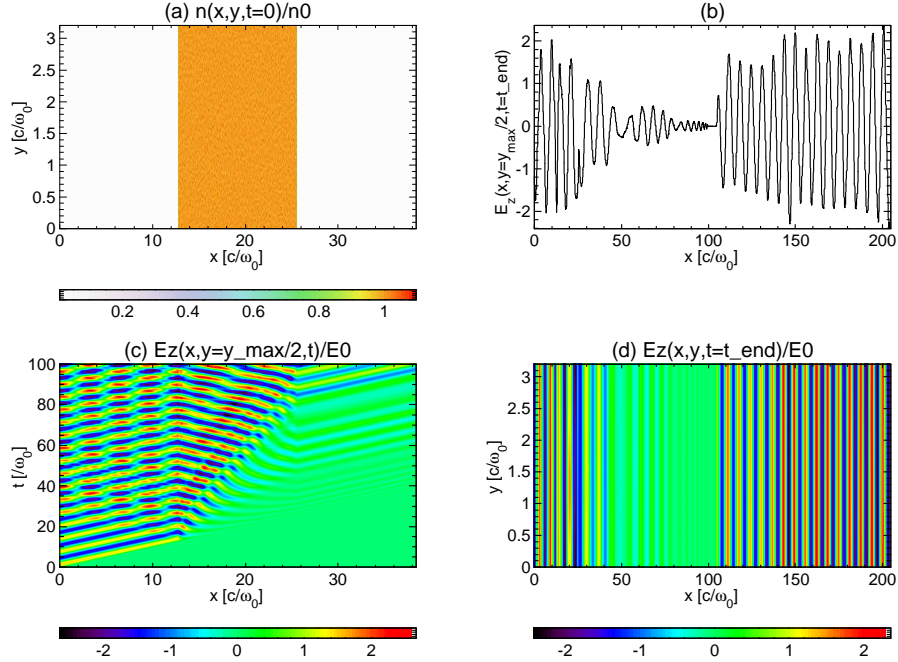


FIG. 2: Case 2: (a) $n(x, y, t = 0)/n_0$, (b) a line profile of $E_z(x, y = y_{\max}/2, t = t_{\text{end}})$, (c) time-distance plot of $E_z(x, y = y_{\max}/2, t)/E_0$, (d) $E_z(x, y, t = t_{\text{end}})/E_0$.

In figure 1(b) we plot the same electric field component but for the case 1b, i.e. when plasma is present, but metamaterial is not. Because plasma is overdense, EM wave with frequency $\omega_0 = \omega_{\text{pe}}/1.5$, cannot propagate through plasma and a standing EM wave forms. In figure 1(c) we plot the same but for

the case 1c, i.e. when plasma is absent ($n_{e,i} = 10^{-2}n_0$), but metamaterial is present. Because metamaterial frequency is $\omega_m = 1.7\omega_0$, the metamaterial μ_m is negative so again EM wave with frequency ω_0 , cannot propagate through plasma-metamaterial region and a standing EM wave forms. In figure

1(d) we plot the same but for the case 1d, i.e. when both plasma and metamaterial are present and form a composite between grid points 512 and 1024 in x -direction. We now see that in the plasma metamaterial composite region which lies in the interval $12.8 < x < 25.6$ EM wave with frequency ω_0 propagates with negative phase speed (and positive group speed) because effective permittivity of the plasma ϵ_p and the effective permeability of the metamaterial μ_m are both negative. We note that our figure 1 matches closely figure 2 from Ref.[1]. Since our simulation parameters for case 1 ($\omega_{pe} = 1.5\omega_0$ and $\omega_m = 1.7\omega_0$) are similar, to that of Ref.[1] hence the similarity of the time-distance plots is successfully achieved. In effect, figure 1 can be regarded as a successful reproduction of 1D results of Ref.[1] now with EPOCH 2D.

Next, in order to study 2D effects in the subsequent runs, for the testing purposes, in case 2 now the grid size is increased in y -direction to 128. That is in case 2 everything else is the same as in case 1d, but grid size is $n_x \times n_y = 8192 \times 128$. In figure 2(a) we show a number density slab of plasma that lies in the intervals $12.8 < x < 25.6$ and it is uniform in y -direction with $0 < y < 3.2$. We note that $n(x, y, t = 0)/n_0$ in these intervals is close to unity, i.e. $n(x, y, t = 0)/n_0 = 1$ – see color table of figure 2(a). In figure 2(b) we plot line profile of electric field $E_z(x, y = y_{\max}/2, t = t_{\text{end}})$ in the middle grid point in y at the final simulation time. Note the different x -range of plots used in figure 2(a) and figure 2(b). In the latter the entire simulation domain length is shown, in the former only the area around plasma-metamaterial composite is presented. The purpose of figure 2(b) is to prove that the electric field of the EM wave that goes in negative x -direction and because of periodic boundary conditions re-appears on the right-side of the domain, does not collide with EM wave that goes in positive x -direction. We consider EM wave that travels in positive x -direction as a main object of our study. The negative x -direction going wave can be regarded as a parasitic wave that cannot be avoided due to imperfect means of EM wave excitation. Essentially figure 2(b) proves that because of the absence of the left-right-travelling EM wave collision, any behaviour for $x > 100$ can be ignored. In figure 2(c) we show time-distance plot of $E_z(x, y = y_{\max}/2, t)/E_0$. We note that this plot is very similar (if not identical) to 1(d). This is because of the uniformness in y -direction of the number density, whether $n_y = 3$ or 128 it makes no difference. The same conclusion follow from figure 2(c) that in the region of plasma metamaterial is present ($12.8 < x < 25.6$) we witness negative phase speed (and positive group speed) EM wave propagation in an over-dense plasma. In figure 2(d) we plot $E_z(x, y, t = t_{\text{end}})/E_0$. The purpose of this plot is to ascertain that no y -variation is seen as the problem is uniform in y -direction. Indeed, we see from figure 2(d) that this is the case.

Cases 3 and 4 aim to study trapping of EM waves by plasma-metamaterial composite barriers. Thus, in case 3 we consider a shallow slab (a barrier) where plasma number density is dropping to $0.8n_0$, while in case 4, number density is dropping to $0.015n_0$, both in the interval between 640 and 896 grid points in x -direction. In the normalized units this is $12.8 \times 640/512 < x < 12.8 \times 896/512$ i.e. $16 < x < 22.4$, which can be seen as light-green color strip in the middle of figure

3(a) and a white color strip in the middle of figure 4(a). In case 3 ($(1 - F) \times 1.5 = 1.2$) plasma metamaterial composite should be transparent to EM wave with negative phase speed propagation, while in case 4 ($(1 - F) \times 1.5 = 0.015$) plasma metamaterial composite should be opaque to the EM wave. That is exactly what we see in figures 3(c) and 4(c): in figure 3(c) the EM wave propagates freely through the entire plasma metamaterial composite ($12.8 < x < 25.6$), while in figure 4(c) EM wave is blocked by the deep density drop $16 < x < 22.4$, hence a standing EM wave forms near the $x = 16$ edge. This way, we achieve trapping of EM wave by dropping density in the plasma metamaterial composite to an appropriate value, such that $(1 - F) \times 1.5 < 1$ condition is met. In figure 3(b) we see similar behaviour of electric field as in 2(b), but figure 4(b) is significantly different, we gather that $E_z(x, y = y_{\max}/2, t = t_{\text{end}})$ amplitude is significantly reduced and the frequency of the EM wave is increased. We conjecture that only non-linear harmonics can tunnel through the density drop which acts as a barrier to negative phase speed propagation seen in figures 2(b,c) figure 3(b,c). For consistency we also check spatial structure of EM wave $E_z(x, y, t = t_{\text{end}})/E_0$ in figures 3(d) and 4(d). Indeed we see in figure 4(d) that EM wave that propagates in the positive x -direction, does not move beyond $x > 16$, as it is effectively trapped.

Cases 5 and 6 also aim to study trapping of EM waves by plasma-metamaterial composite, but instead of a slab we consider two-dimensional density rectangular depletions (DRD) that can be seen in figures 5(a) and 6(a), as light-green and white color boxes. In them, the number density drops to $0.8n_0$ in case 5 (as in case 3) and $0.015n_0$ in case 6 (as in case 4). Their dimensions are $x_{\text{rect}} = 22 - 16 = 6$ and $y_{\text{rect}} = 0.64 \approx 1$ i.e. $y_{\text{rect}} \approx c/\omega_0$. The gaps between DRDs are 0.32, i.e. $\approx (1/3) \times (c/\omega_0)$. Essentially, we wanted to add some structuring in y -direction with structures on the scale of EM wave inertial length of $\approx c/\omega_0$. The results of the last two entries from table I are shown in figures 5 and 6. We gather from figures 5 and 6 that shallow DRDs are transparent to EM wave, while deep ones block EM wave, as expected. Next, we focus our attention on the differences from cases 3 and 4, presented earlier in figures 3 and 4. It can be seen in figure 6(b) that electric field from has complex beating pattern (multiple harmonic beating). This is in contrast to figure 4(b) where high frequency harmonics show a regular spatial pattern (no beats). Figure 6(d) does not show any structuring in y -direction, which seems somewhat counter intuitive. As, for example, it seems not clear at first sight, why in-between DRDs across y -coordinate where normalized plasma number density is unity, i.e. in the four light-brown color strips on top and bottom of white rectangles in figure 6(a), no clear EM wave propagation seen. Our explanation is that shortness of the considered gaps, $\approx (1/3) \times (c/\omega_0)$, is not sufficient for apparent EM wave front propagation as the wave interacts with plasma on circa $> c/\omega_0$ scale. Nonetheless, the beats are seen in 6(b), which means there is some propagation in the gaps, hence the beat pattern. Ideally, in retrospect, we surmise that a bigger than $n_y = 128$ could have been considered. Nonetheless, we still think the considered y -coordinate structuring in cases 5 and 6 provide a useful information. Future, a more elaborate

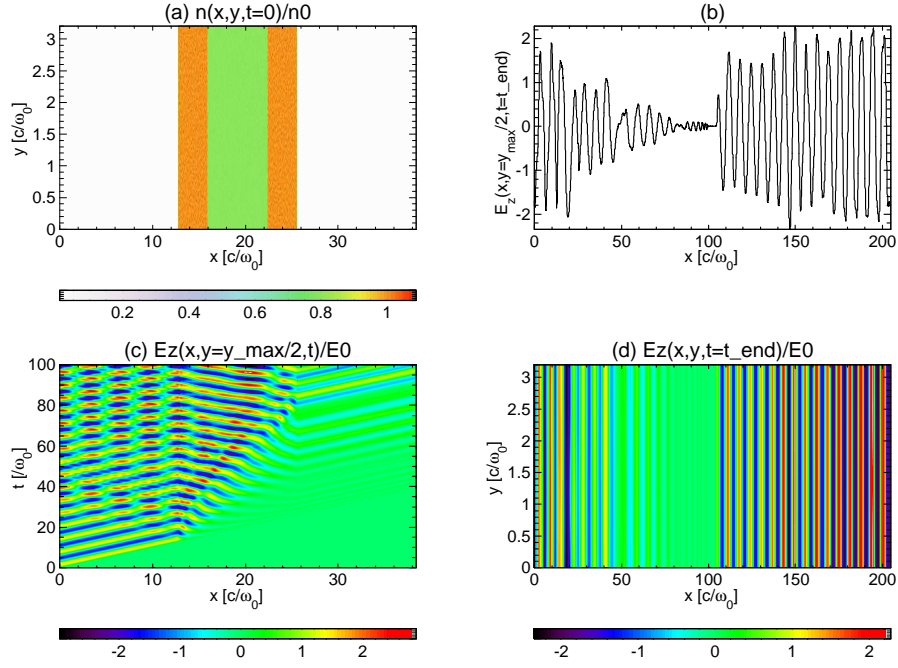


FIG. 3: The same as in figure 2, but now for case 3.

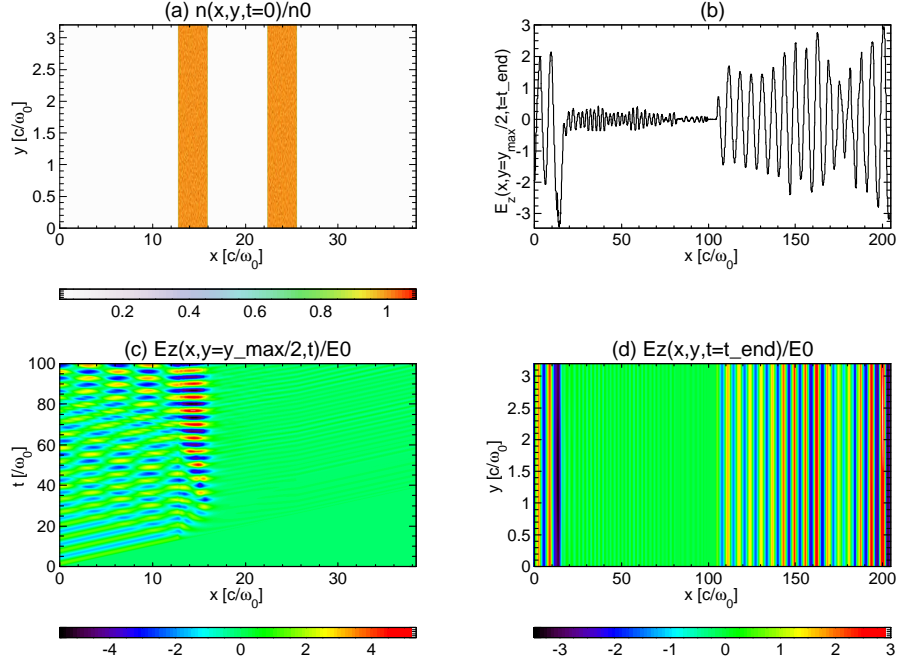


FIG. 4: The same as in figure 2, but now for case 4.

study, could potentially consider different shapes of DRDs and different separation distances, which could be a subject to next work(s).

IV. SUMMARY AND CONCLUSIONS

The aim of this work is two-fold: (i) to extend previous 1D studies [1] of electromagnetic (EM) waves propagation in an over-dense plasma-metamaterial composite into 2D spatial dimensions and (ii) to study trapping of EM waves by the composite 2D structures that act like barriers, which is analogous

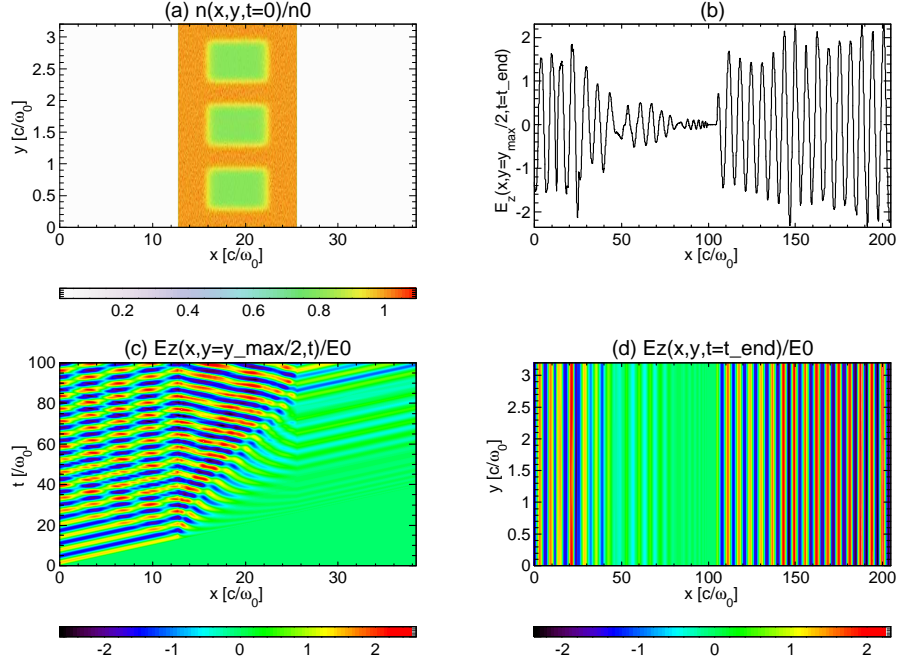


FIG. 5: The same as in figure 2, but now for case 5.

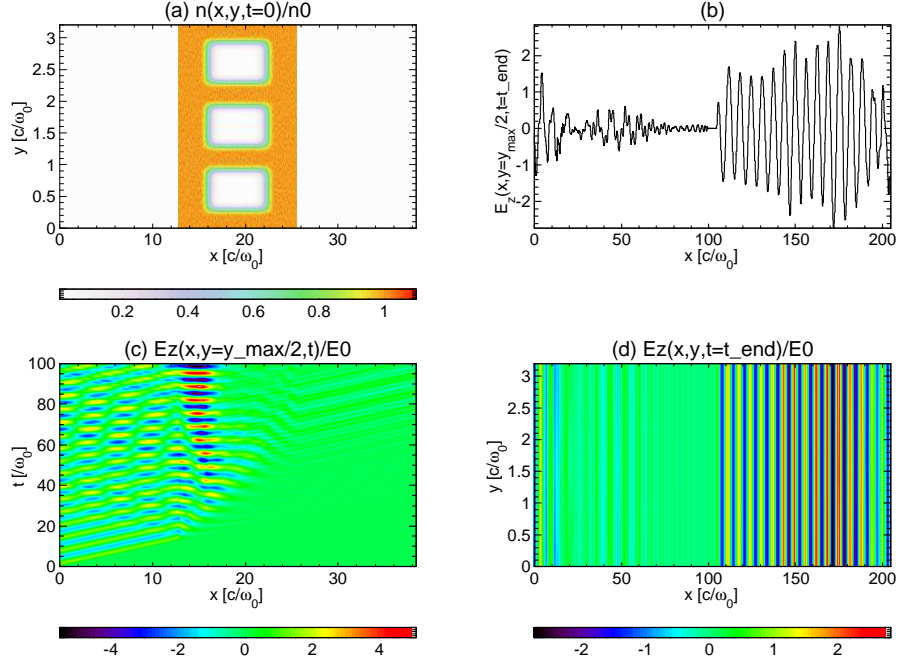


FIG. 6: The same as in figure 2, but now for case 6.

to EM wave trapping by preformed density cavities in near-critical density plasmas [29]. Our study comprises of several logical steps:

1. In Appendix A we presented a numerical recipe how to include the presence of metamaterial in plasma by adding additional current J_m using EPOCH 2D PIC code.
2. We then validated the modification of EPOCH code (fig-

ure 1, cases 1a, 1b, 1c and 1d, see table I) by a successful reproduction of 1D results of Ref.[1] with EPOCH 2D on a $n_x \times n_y = 8192 \times 3$ grid.

3. With a purpose to study 2D effects in this work, in case 2 we increased grid size y -direction to 128 and ascertained negative phase speed propagation (figure 2(c)) which is nearly identical to figure 1(d) (the quasi-1D case with $n_y = 3$ grids

along y-axis).

4. Next, we wanted to study EM wave trapping by a slab of density depletion (cases 3 and 4). Thus, we set plasma number density according to equation (7). We find that in case 3 $((1 - F) \times 1.5 = 1.2)$ plasma metamaterial composite is transparent to EM wave. In this case EM wave propagates with a negative phase speed, while in case 4 $((1 - F) \times 1.5 = 0.015)$ plasma metamaterial composite is opaque to the EM wave. Thus, forming a standing wave at the edge of an opaque region. Here the generic conclusions are as following: (i) if $(1 - F) \times n_0$ is the minimal number density of the plasma slab and (ii) $f = \omega_{pe}/\omega_0$ is the factor by which EM wave's angular frequency ω_0 is less than electron plasma frequency ω_{pe} , then the condition for EM wave trapping by the slab is

$$(1 - F) \times f < 1. \quad (9)$$

We also find that when condition given by equation (9) is met, EM amplitude is significantly reduced and the frequency of the EM wave is increased (figure 4(b)). This leads to a conclusion that only non-linear harmonics can tunnel through the density drop which acts as a barrier to negative phase speed propagation found in figures 2(b,c) figure 3(b,c).

5. Further, we aimed to study EM wave trapping by two-dimensional DRDs (cases 5 and 6). Therefore plasma number density was set according to equation (8). We find that for the sizes and shapes of DRDs considered, behaviour is similar to the plasma slab density depletion. The main difference is that electric field from. It now has complex beating pattern (figure 6(b)). Such behaviour is in contrast to figure 4(b), where where high frequency harmonics show a regular spatial pattern and no beats are present. For two-dimensional DRDs the EM wave trapping condition is also given by equation (9).

In summary, the barriers for EM wave propagation are created when metamaterial spatially co-exists with a plasma density depletion in a form of a slab or two-dimensional DRDs. Such approach is analogous to EM wave trapping by preformed density cavities in near-critical density plasmas investigated by Ref. [29]. We have shown that plasma metamaterial composite allows to trap EM waves by both a slab (figure 4(c)) and DRD configurations (figure 6(c)). In both cases a standing wave at the edge of an opaque region is formed. The EM wave trapping condition is established by equation (9), which is supported by our PIC numerical simulations. In our approach metamaterial *acts like an agent that lets EM wave to enter over-dense plasma*. The subsequent density drop *makes plasma opaque to the EM wave*, effectively trapping it in form of a standing wave at the edge of the barrier (density depletion slab or two dimensional DRDs).

Ref. [29] established that in a situation when a near-critical density plasma contains a preformed density cavity, EM wave is trapped and becomes a standing wave. Their 2D PIC simulations have shown that within $100 - 200/\omega_0$ the standing wave damps away. We only show numerical results with end simulation time of $100/\omega_0$, but confirm similar result to Ref. [29] that within few hundred $1/\omega_0$ EM wave indeed damps. We suggest that the wave damping can offer applications such as heat deposition or substrate materials (micro)machining [32] depending on EM wave intensity. Low intensity EM waves

would simply heat the plasma, potentially, high intensity EM waves can be used for substrate materials (micro)machining. From figure 4(c) (density depletion slab case) and figure 6(c) (two-dimensional DRDs case) we see that length scale of the standing wave pattern is $(1 - 2)c/\omega_0 = 0.25 - 0.5$ m. Obviously this is the value for $n_0 = 10^{15}$ particles per m^{-3} used, because number density sets $\omega_{pe} = 1.784 \times 10^9$ Hz rad, which, in turn, sets $\omega_0 = \omega_{pe}/1.5 = 1.189 \times 10^9$ Hz rad. Setting higher number density say $n_0 = 10^{19} m^{-3}$, can make c/ω_0 as small as 2.5 mm. Our results potentially suggest yet unexplored applications such as: more efficient plasma vapour deposition (because the reaction rate is proportional to the product of number densities of the reactant species), controlling EM wave propagation (EM wave trapping) in invisibility cloaks and similar.

There are many examples when there is a good reason to conduct multi-scale numerical simulations combining ab initio/density functional theory/molecular dynamics-type simulations [33] and meso-scale, particle-in-cell-based modelling, such as: (i) correlated simulation studies concerning plasma charging and its effects over ten orders of magnitude in length scales at the lunar terminator [34], (ii) dynamic coupling between particle-in-cell and atomistic simulations to simulate metal surface response to high electric fields [35], (iii) molecular dynamics model and particle-in-cell model to investigate the physics of ionic electrospray propulsion over 9 orders of magnitude in length scale [36], (iv) multi-scale/hybrid modelling of low temperature plasmas for fundamental investigations and equipment design [37], (v) gas discharge plasmas used for various materials science applications [38]. Future extensions of this work will be combining molecular dynamics and particle-in-cell modeling as e.g. in Ref.[35].

DATA AVAILABILITY

The data and numerical codes that support the findings of this study are available from the corresponding author upon reasonable request.

Appendix A: Appendixes

Here we present a numerical recipe how to include the presence of metamaterial in plasma by adding the additional current J_m using EPOCH PIC code [24]. The latter can be downloaded from GitHub repository <https://epochpic.github.io/quickstart.html>.

Step 1: edit `src/epoch2d.F90` and after line

```
CALL open_files      ! setup.f90
```

```
initialize Jm,y as zero value
```

```
jmy(:,:) = 0.0_num.
```

Note that "underscore num" is making sure that EPOCH is using F90 double precision, which is EPOCH's default accuracy. Historically using the compiler auto-promotion of

REAL to DOUBLE PRECISION was unreliable, so EPOCH uses "kind" tags to specify the precision of the code. See section 1.5 in the EPOCH user manual.

Step 2: edit

```
src/shared_data.F90
```

and in the following line add $J_{m,y}$ declaration (last entry):

```
REAL(num), ALLOCATABLE, DIMENSION(:, :) :: &  
ex, ey, ez, bx, by, bz, jx, jy, jz, jmy
```

Step 3: edit

```
src/housekeeping/mpi_routines.F90
```

and after line 388 add

```
ALLOCATE(jmy(1-jng:nx+jng, 1-jng:ny+jng))
```

to allocate $J_{m,y}$ array.

Step 4: edit src/fields.f90 and after line "CONTAINS" add two following subroutines in the case of both plasma and metamaterial composite are present. If metamaterial is absent and only electric field of EM wave needs to be driven, then only leave the 1st subroutine. Below are the said two subroutines:

```
SUBROUTINE drive_field(time)  
REAL(num), INTENT(IN) :: time  
IF (x_min_boundary) THEN  
  ez(1,:) = ez(1,:) + 760199.13_num*&  
  sin(1.1893397e+09_num*time)  
END IF  
END SUBROUTINE drive_field
```

```
SUBROUTINE drive_mfield(time)  
REAL(num), INTENT(IN) :: time
```

```
IF (x_min_boundary) THEN  
  jmy(512:1024,:) = jmy(512:1024,:) + hdt*&  
  (1.7_num*1.1893397e+09_num)**2*by(512:1024,:)&  
  by(512:1024,:) = by(512:1024,:) -&  
  hdt*jmy(512:1024,:)&  
END IF  
END SUBROUTINE drive_mfield
```

Further, in the end of src/fields.f90 file, after half-time step and full time step the following calls to the said routines should be added:

```
CALL update_e_field  
CALL drive_field(time+0.5_num*dt)  
CALL efield_bcs  
CALL update_b_field  
CALL drive_mfield(time+0.5_num*dt)  
...  
CALL update_b_field  
CALL drive_mfield(time+dt)  
CALL bfield_final_bcs  
CALL update_e_field  
CALL drive_field(time+dt)  
CALL efield_bcs
```

Note that there is no need to modify EM solver part in the src/fields.f90 file. The fact that presence of metamaterial is implemented by setting J_m as in the above subroutine `jmy(512 : 1024, :)` puts a *restriction* on number of processors that can be used in x -direction. The grid cells 512 : 1024 must fit on the first processor. Thus, because $8192/1024 = 8$, we are restricted to use no more than 8 processors in x -direction. There is no restriction on number of processors in y -direction. EPOCH code allows simulation domain decomposition to be set manually. In this work we have used EPOCH's `nprocx=8` and `nprocy=1` setting.

-
- [1] A. Iwai, O. Sakai, and Y. Omura, *Physics of Plasmas* **24**, 122112 (2017).
 - [2] M. A. Lieberman and A. J. Lichtenberg, *Principles of Plasma Discharges and Materials Processing* (Wiley, Hoboken, 1994).
 - [3] N. Selvakumar and H. C. Barshilia, *Solar Energy Materials and Solar Cells* **98**, 1 (2012).
 - [4] J. Hanlon and R. J. Kelsey, *Handbook of Package Engineering* (CRC Press, Boca Raton, 1998).
 - [5] E. Fortunato, P. Barquinha, and R. Martins, *Advanced Materials* **24**, 2945 (2012).
 - [6] H. Sugai, I. Ghanashev, and M. Nagatsu, *Plasma Sources Science and Technology* **7**, 192 (1998).
 - [7] V. G. Veselago, *Soviet Physics Uspekhi* **10**, 509 (1968).
 - [8] J. Pendry, A. Holden, D. Robbins, and W. Stewart, *IEEE Transactions on Microwave Theory and Techniques* **47**, 2075 (1999).
 - [9] R. W. Ziolkowski and E. Heyman, *Phys. Rev. E* **64**, 056625 (2001).
 - [10] S. Foteinopoulou, E. N. Economou, and C. M. Soukoulis, *Phys. Rev. Lett.* **90**, 107402 (2003).
 - [11] V. M. Agranovich, Y. R. Shen, R. H. Baughman, and A. A. Zakhidov, *Phys. Rev. B* **69**, 165112 (2004).
 - [12] I. V. Shadrivov, A. A. Zharov, and Y. S. Kivshar, *J. Opt. Soc. Am. B* **23**, 529 (2006).
 - [13] R. Boyd, *Nonlinear Optics, 3rd ed.* (Elsevier, London, 2008).
 - [14] R. A. Shelby, D. R. Smith, and S. Schultz, *Science* **292**, 77 (2001).
 - [15] A. A. Houck, J. B. Brock, and I. L. Chuang, *Phys. Rev. Lett.* **90**, 137401 (2003).
 - [16] C. G. Parazzoli, R. B. GREGOR, K. Li, B. E. C. Koltenbah, and M. Tanielian, *Phys. Rev. Lett.* **90**, 107401 (2003).
 - [17] W. Rotman, *IRE Transactions on Antennas and Propagation* **10**, 82 (1962).
 - [18] Y. Nakamura and O. Sakai, *Japanese Journal of Applied Physics* **53**, 03DB04 (2014).
 - [19] A. Iwai, Y. Nakamura, A. Bambina, and O. Sakai, *Applied Physics Express* **8**, 056201 (2015).
 - [20] A. Iwai, Y. Nakamura, and O. Sakai, *Phys. Rev. E* **92**, 033105 (2015).
 - [21] O. Sakai, *Journal of Applied Physics* **109**, 084914 (2011).
 - [22] K. Kourtzanidis, D. M. Pederson, and L. L. Raja, *Journal of Applied Physics* **119**, 204904 (2016).
 - [23] A. Iwai, Y. Nakamura, O. Sakai, and Y. Omura, *Plasma Sources*

- Science and Technology **29**, 035012 (2020).
- [24] T. D. Arber, K. Bennett, C. S. Brady, A. Lawrence-Douglas, M. G. Ramsay, N. J. Sircombe, P. Gillies, R. G. Evans, H. Schmitz, A. R. Bell, and C. P. Ridgers, Plasma Physics and Controlled Fusion **57**, 113001 (2015).
 - [25] M. Y. Yu, P. K. Shukla, and K. H. Spatschek, Phys. Rev. A **18**, 1591 (1978).
 - [26] X. Wang, W. Yu, M. Y. Yu, H. Xu, J. W. Wang, and X. Yuan, Physics of Plasmas **16**, 053107 (2009).
 - [27] S. Luan, W. Yu, W. Xu, M. Murakami, H. Zhuo, J. Wang, X. Wang, and H. Wu, Applied Physics B **108**, 875 (2012).
 - [28] B. Zhu, Y.-C. Wu, K.-G. Dong, W. Hong, J. Teng, W.-M. Zhou, L.-F. Cao, and Y.-Q. Gu, Physics of Plasmas **19**, 102304 (2012).
 - [29] S. Luan, W. Yu, J. Wang, M. Yu, S. Weng, M. Murakami, J. Wang, H. Xu, and H. Zhuo, Laser and Particle Beams **31**, 589 (2013).
 - [30] D. Tsiklauri, Research in Astronomy and Astrophysics **24**, 095021 (2024).
 - [31] E. Esarey, C. B. Schroeder, and W. P. Leemans, Rev. Mod. Phys. **81**, 1229 (2009).
 - [32] B. Stockdale, JALA: Journal of the Association for Laboratory Automation **4**, 35 (1999).
 - [33] S. Jenkins and I. Morrison, Chemical Physics Letters **317**, 97 (2000).
 - [34] J. Wang and Z. Huang, IEEE Transactions on Plasma Science **51**, 2561 (2023).
 - [35] M. Veske, A. Kyritsakis, F. Djurabekova, K. N. Sjobak, A. Aabloo, and V. Zadin, Phys. Rev. E **101**, 053307 (2020).
 - [36] J. Asher, Z. Huang, C. Cui, and J. Wang, Journal of Applied Physics **131**, 014902 (2022).
 - [37] M. J. Kushner, Journal of Physics D: Applied Physics **42**, 194013 (2009).
 - [38] A. Bogaerts, K. De Bleecker, V. Georgieva, I. Kolev, M. Madani, and E. Neyts, Plasma Processes and Polymers **3**, 110 (2006).